HHS Public Access

Author manuscript

J Control Release. Author manuscript; available in PMC 2018 February 28.

Published in final edited form as:

J Control Release. 2017 February 28; 248: 53–59. doi:10.1016/j.jconrel.2017.01.008.

Regeneration of bone using nanoplex delivery of FGF-2 and BMP-2 genes in diaphyseal long bone radial defects in a diabetic rabbit model

Behnoush Khorsand, **Nate Nicholson**, **Anh-Vu Do**, **John E. Femino**, **James A. Martin**, **Emily Petersen**, **Brian Guetschow**, **Douglas C. Fredericks**, and **Aliasger K. Salem**

Abstract

Bone fracture healing impairment related to systemic diseases such as diabetes can be addressed by growth factor augmentation. We previously reported that growth factors such as fibroblast growth factor-2 (FGF-2) and bone morphogenetic protein-2 (BMP-2) work synergistically to encourage osteogenesis *in vitro*. In this report, we investigated if BMP-2 and FGF-2 together can synergistically promote bone repair in a leporine model of diabetes mellitus, a condition that is known to be detrimental to union. We utilized two kinds of plasmid DNA encoding either BMP-2 or FGF-2 formulated into polyethylenimine (PEI) complexes. The fabricated nanoplexes were assessed for their size, charge, *in vitro* cytotoxicity, and capacity to transfect human bone marrow stromal cells (BMSCs). Using diaphyseal long bone radial defects in a diabetic rabbit model it was demonstrated that co-delivery of PEI-(*pBMP-2*+*pFGF-2*) embedded in collagen scaffolds resulted in a significant improvement in bone regeneration compared to PEI-*pBMP-2* embedded in collagen scaffolds alone. This study demonstrated that scaffolds loaded with PEI-(*pBMP-2*+*pFGF-2*) could be an effective way of promoting bone regeneration in patients with diabetes.

Graphical abstract

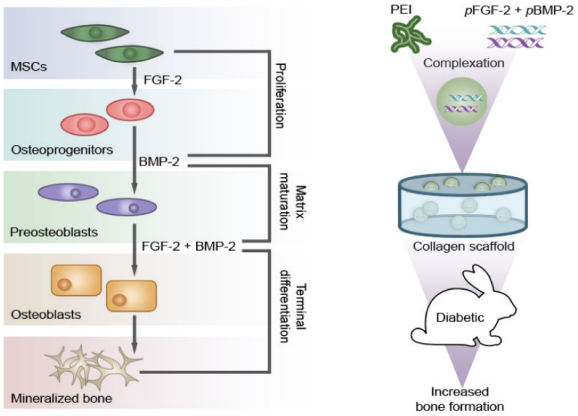

Keywords

Bone morphogenetic protein-2 (BMP-2); Fibroblast growth factor-2 (FGF-2); Diabetes mellitus; Polyethylenimine; Non-viral gene delivery; Bone regeneration

1. Introduction

Certain systemic diseases capable of impairing glucose metabolism can have profound deleterious effects on bone metabolism and bone healing [1]. Chronic diabetes mellitus (DM) is associated with decreased bone mineral density [2] and increased risk of fractures [3]. Individuals with DM have a significantly increased fracture risk compared with non-diabetic individuals [4]. Furthermore, they have an increased incidence of non-union after fracture, delayed union, and pseudarthrosis [5, 6]. Several animal studies have documented that the animals with spontaneous DM or chemically induced DM have impaired callus formation as illustrated by reduced material strength properties of the callus compared with matched controls [7-10]. The cause of the altered biology at a diabetic fracture site remains unknown but is likely to be multifactorial with factors such as protein deficiency, neuropathy, small vessel deficiency [11] and increased rates of cartilage resorption all being potential contributors [12]. The necessity for better therapeutics stimulating bone regeneration and the healing of fractures in patients with chronic systemic conditions such as DM has resulted in the introduction of novel biomaterials, biomimetic factors, custom-fit printed scaffolds and cell based approaches in medicine [13]. One such development is the current clinical use of locally applied recombinant proteins that include bone morphogenetic protein-2 (BMP-2) or fibroblast growth factor-2 (FGF-2) for promoting osteogenesis. There have been a few studies that have explored the effect of locally applied recombinant human BMP-2 and FGF-2 to achieve bone regeneration in DM [14, 15] and non-DM bone defect models [16-18]. It has been shown that BMP-2 treatment of fractures in a diabetic setting increased callus formation, vascularity and mechanical properties [14]. It has also been reported that intermittent FGF-2 treatment increased expression of transforming growth factor-beta (TGF-β) and increased callus formation at a fibula fracture site in diabetic rats [15].

BMP-2 is member of the TGF-β superfamily, which mediates multiple biological processes including regulation of bone formation [19]. BMP-2 is produced by osteoblastic cells and transduces its signals into the nucleus by binding to type I receptors (BMPR I) that then recruit type II receptors (BMPR II). BMP receptors then propagate their signals by phosphorylating several SMAD proteins (SMAD1, 5 or 8), which leads to upregulation of runt-related transcription factor 2 (Runx2)[20]. In addition, FGF-2 is also highly expressed in osteoblasts which modulates the proliferation and differentiation of mesenchymal stem cells [21]. FGF-2 signals through FGF receptor tyrosine kinases (FGFR1 to FGFR4). In osteoblasts, the interactions between FGF-2 and its receptors induces autophosphorylation of the receptors, which in turn activates and recruits FRS2 [22], src, ras, raf and extracellular signal-related kinase (ERK) [23], which leads to an increase in *Runx2* transcription [24]. Runx2 is a critical transcription factor in osteoblast precursor proliferation and differentiation [25]. Activation of Runx2 leads to increased expression of osteoblast-specific

proteins, such as alkaline phosphatase and osteocalcin at different stages of osteogenesis, both of which promote bone formation [26]. *In vivo*, multiple growth factors act synergistically toward their respective target cells. For example, there is cooperation between BMP-2 and FGF-2 which act synergistically to enhance osteogenesis by promoting Runx2 transcription, through the activation of SMAD and ERK signaling pathways [27]. Our previous study revealed the synergistic effect on osteogenesis of the combinatorial treatment of *BMP-2* and *FGF-2 in vitro* [28]. Recombinant human protein growth factor based therapies have observable therapeutic effects. However, recombinant human proteins are expensive to manufacture and due to their short half-lives, there is a need for supraphysiological dosages for them to be clinically effective [29]. It has been shown that such high doses of recombinant human protein is associated with several side effects such as soft tissue swelling and ectopic bone formation [30]. Non-viral gene therapy is a promising alternative to protein based therapies [31]. It was shown that non-viral delivery of *BMP-2* and *FGF-2* genes enhanced upregulation of *Runx2* and *osteocalcin* transcription, which led to significantly enhanced mineralization in transfected cells versus non-transfected controls [28].

To our knowledge, no published study exists examining the synergistic effect of non-viral gene delivery of plasmids independently encoding BMP-2 and FGF-2 on the promotion of fracture healing in a chronic diabetic animal model. We hypothesized that non-viral gene delivery of *BMP-2* and *FGF-2* will synergistically attenuate the deleterious effects of DM on healing at the bone defect site. In the present study, well characterized nanoplexes were prepared by utilizing a cationic polymer, polyethylenimine (PEI), to condense plasmid DNA encoding BMP-2 and FGF-2 through electrostatic interaction. It has been previously shown that these nanoplexes possess efficient transfection capability both *in vitro* [28] and *in vivo* [32]. Collagen scaffolds harboring PEI-(*pBMP-2*+*pFGF-2*) nanoplexes, improved bone regeneration rates and increased callus formation when implanted into rabbit radius metaphyseal defect sites compared to control groups.

2. Materials and methods

2.1. Materials

Alloxan monohydrate, branched PEI (mol. wt. 25 kDa) and the GenElute™ HP endotoxin-free plasmid maxiprep kit were purchased from Sigma-Aldrich® (St. Louis, MO). The BMP-2 ELISA kit was purchased from Quantikine® (R & D Systems®, Minneapolis, MN). Plasmid DNA (6.9 Kb) encoding BMP-2 protein (Catalog number: SC119392) and plasmid DNA (4.9 Kb) encoding basic fibroblast growth factor-2 protein (FGF-2) (Catalog number: SC118884) were purchased from Origene Technologies, Inc. (Rockville, MD). Human bone marrow stromal cells (BMSCs) were purchased from the American Type Culture Collection (ATCC®, Manassas, VA). Dulbecco's Modified Eagle's Medium (DMEM), trypsin-EDTA (0.25%, 1X solution) and Dulbecco's phosphate buffered saline (PBS) were purchased from Gibco® (Invitrogen™, Grand Island, NY). Fetal bovine serum (FBS) was obtained from Atlanta Biologicals® (Lawrenceville, GA). Gentamycin sulfate (50 mg/ml) was purchased from Mediatech Inc. (Manassas, VA). Absorbable type-I bovine collagen was provided from Zimmer Dental Inc. (Carlsbad, CA). MTS cell proliferation assay reagent (Cell Titer 96

AQueous One Solution Cell Proliferation Assay) was purchased from Promega (Madison, WI).

2.2. Isolation of plasmid DNA (pDNA) encoding BMP-2, and FGF-2 and fabrication and characterization of PEI-pDNA nanoplexes

Competent *E. coli* DH5α™ were transformed with the relevant *pDNA* which was subsequently amplified, purified and analysed for purity as previously described [33]. Nanoplexes were created at a molar ratio of PEI amine (N) to *pDNA* phosphate (P) groups of 10, to achieve optimal transfection efficacies [33]. PEI-*pDNA* nanoplexes were formed by mixing 500 μL PEI solution with 500 μL *pDNA* (*pBMP-2 or pFGF-2*) solution containing 50 μg *pDNA* and vortexing for 30 s. A 1 ml solution of *pFGF-2* and *pBMP-2* plasmids containing 50 μg of each plasmid was mixed well by vortexing, and 500 μL was added to a separate vial. Then 500 μL of an indicated PEI concentration was added to the 500 μl of plasmid solution and vortexed for 30 s. The final mixture, containing 25 μg of *pFGF-2* and 25 μg of *pBMP-2*, was incubated for 30 min at ambient temperature to permit the formation of complexes through electrostatic interaction between PEI (amine groups) and *pDNA* (phosphate groups). A volume of 20 μl (containing 1 μg *pDNA*) of theses complexes was subsequently used for biocompatibility and *in vitro* transfection experiments. Nanoplexes in water were characterized for their size and zeta-potential using a Zetasizer Nano-ZS (Malvern Instruments, Westborough, MA) as previously described [34].

2.3. Collagen scaffold characterization

Collagen scaffold surface morphology was studied using scanning electron microscopy (SEM, Hitachi Model S-4800, Japan). Briefly, the scaffolds were mounted on a SEM aluminum stub using double stick carbon tape. This was sputter-coated with gold-palladium using an argon beam K550 sputter coater (Emitech Ltd., Kent, England). Images were captured using the Hitachi S-4800 SEM operated at 3 kV accelerating voltage and a current of 10 lA.

2.4. Fabrication of nanoplex-embedded collagen scaffolds

After preparation of nanoplexes at N/P ratio of 10, the nanoplexes were injected, using a sterile 28 gage needle, into the collagen scaffolds (hand cut into 5 mm × 5 mm). Afterwards, the nanoplex-embedded collagen scaffolds were lyophilized.

2.5. Cell culture

BMSCs were maintained in DMEM supplemented with 10% FBS and 1% gentamycin (50 μg/ml) in a humidified incubator (Sanyo Scientific Autoflow, IR direct heat CO_2 incubator) at 37°C containing 95% air and 5% CO_2. Cells were cultured on 75 cm^2 polystyrene cell culture flasks (Corning, NY, USA) and sub-cultured (sub-cultivation ratio of 1:9) after 80–90% confluence was achieved. BDMCs were used in experiments at passage numbers 4 – 6.

2.6. Assessment of cytotoxicity and transfection efficiency of PEI-pDNA (pBMP-2 and pFGF-2) nanoplexes in vitro using BMSCs

Cytotoxicity of *PEI-pDNA* nanoplexes, at the N/P ratio of 10, cultured with BMSCs was assessed with the Cell Titer 96 AQueous One Solution cell proliferation assay as described previously [34]. Each treatment was performed at n = 6. For measuring transfection efficiencies BMSCs, seeded into 24-well plates at 80,000 cells/well the previous day, were treated with 20 μl (1 μg *pDNA*) of complexes (N/P ratio of 10) in the presence of serum-free medium. Controls included untreated cells and cells treated with PEI alone. After an incubation of 4 h, the serum-free medium was replaced with growth medium containing serum. At 48 h post transfection, heparin (10 mg/ml) was added to BMSCs for 4 h to prevent the retention of BMP-2 and FGF-2 on the cell surface membrane of BMSCs. The supernatants were collected and analyzed using an ELISA kit, to quantify the amount of the BMP-2 and FGF-2 protein secreted. Mean values were recorded from n = 4 measurements.

2.7. Induction and Management of Diabetes mellitus in a rabbit model

A rabbit model of type 1 diabetes mellitus was created by using alloxan as described elsewhere [35]. In brief, to induce diabetes, New Zealand male white rabbits (7 months old, 3-4 Kg, Covance, Princeton, NJ) were treated with 100 mg/kg of alloxan solution (5% W/V) by intravenous administration. Following alloxan injection, 10 mL of glucose (5% W/V) was introduced subcutaneously at 4, 8, and 12 h. In addition, an oral solution of glucose (20%) in tap water was provided for 2 days. Their blood glucose levels were monitored every 1-2 h until 12 h post injection. Rabbits blood glucose levels were checked 2 times daily and their weights were recorded twice weekly throughout the study. All animal protocols were performed according to the guidelines provided by the University of Iowa Institutional Animal Care and Use Committee, Iowa.

2.8. Production of metaphyseal tibia/radius defects and implantation of nanoplex-embedded collagen scaffolds

At 6 months following stable diabetes mellitus, the animals were sedated and placed under general anesthesia. The induction group underwent a surgically induced bone void in both radii. Using volar approach, the radial diaphysis was exposed through a 1.5 cm-long incision. The periosteum was dissected off from the proximal to the distal site of the radius. Then a spatula was placed between the radius and ulna to ensure the ulna did not sustain damage as the ulna is the primary weight bearing bone in the rabbit. Using an oscillating saw, a 10 mm defect was generated on the both radii. Then the following treatments were hand-packed into the defect to the level of the original cortex: 1) PEI-*pBMP-2* nanoplex-loaded collagen scaffolds (n=5); 2) PEI-*pFGF-2* nanoplex-loaded collagen scaffolds (n=4); and 3) PEI-(*p*B*MP-2*+*pFGF-2*) nanoplex-loaded collagen scaffolds (n=11). Where appropriate, the scaffolds were cut into cylinders (radius = 5 mm) and a height of 5 mm and the PEI nanoplex solution was introduced into each scaffold and then the scaffolds were implanted into rabbits. Silk sutures were used to close the incision and appropriate approved analgesics were administered intramuscularly to manage the pain. Rabbits were sacrificed after 28 days, and the defect areas were excised from the radial bone and fixed in 10% formalin for subsequent analyses.

2.9. Micro-computed tomography (μCT) studies

Standard craniocaudal and lateral radiographs were obtained of each tibia and radius using a Simon DR Digital x-ray unit (Baltimore, MD). Bone volume (BV) and bone union in the bone defect were quantified using three-dimensional x-ray micro-computed tomography (μCT) imaging. High resolution Skyscan 1176 (Kontich, Belgium) at 9 μm resolution (80 KeV, 313 μA with a voxel size of 12.16 μm, 280 ms exposure) was utilized to obtain the μCT images of the defects. The whole regenerated bone, including a total of 794 reconstructed slices, was analyzed. Using the manufacturer's software (threshold = 0 to 0.03) approximately 18 micron of each defect in the specimen was analyzed. Subsequently, radiographs were evaluated for nascent bone formation in the defect (BV) and the defect healing (union). BV was calculated using the μCT software and union was calculated based on observation of new bone formation bridging with host bone on both sides of the defect.

2.10. Histological observation of Diabetes mellitus rabbit bone samples

The specimens were fixed in 10% neutral buffered formalin, decalcified, dehydrated using increasing concentrations of ethanol, and then treated with xylene (Merck, Germany), and embedded in paraffin. Sagittal sections (5 μm thick) were made in the central part of the wound and samples were collected on Superfrost Plus Slides (Fisher Scientific, Pittsburgh, PA). Sections were deparaffinized and stained with Hematoxylin-Eosin (H&E) and Masson's trichrome. One section, representing the defect area of each as well as undamaged native bone margins on either side of the defects, was used to assess nascent formation of bone and bridging of the defect. All static histomorphometry analyses were performed according to standard protocols by using the OsteoMeasure XP (OsteoMetrics, Inc., Atlanta, GA).

2.11. Statistical analysis

Numerical data are represented as mean (±SEM). All statistical analyses were performed using statistical and graphing software, GraphPad Prism version 6 for windows (GraphPad Software Inc., San Diego, CA). Unless stated otherwise one-way ANOVA analysis of variance followed by Tukey's multiple comparison post-test was used to compare all groups pair-wise. p-values ≤ 0.05 were considered significant.

3. Results and discussion

3.1. Morphology, size and zeta-potential of nanoplexes

The PEI-*p*DNA nanoplexes (N/P ratio of 10) were prepared through electrostatic condensation as described above. The size of nanoplexes ranged from 80 to 117 nm with a narrow size distribution (Table 1). The zeta potential of nanoplexes was in the range of +30 to +35 mV (Table 1). TEM images of PEI-(*pBMP-2*+*pFGF-2*) nanoplexes revealed discrete, spherical particles (fig 1a). The small size and the positive zeta-potential of the complexes are considered to be important characteristics if they are to enter into cells by clathrin-mediated endocytosis [36]. Their positive surface charge can also result in a proton sponge effect, facilitating their release from endolysosomes into cytoplasm [37, 38].

3.2. Analysis of collagen scaffolds by SEM

Using SEM, the 3D collagen scaffolds were characterized. The SEM images demonstrated highly interconnecting porous structures of non-loaded collagen scaffolds (pore diameters ~200 μm) (fig. 1b). Consistent with our previous observations, embedding of nanoplexes within collagen scaffolds did not affect the physico-chemical characteristics of the collagen scaffold [33]. The three-dimensional (3D) porous scaffold creates and maintains a 3D space within the defect *in vivo* and provide a framework for growth of new tissue that eventually replace the scaffold. The scaffold not only provides a supporting matrix for the recruitment of bone cells, but also provides an essential environment for cells to spread, migrate, multiply and differentiate into specific lineages [39, 40].

3.3. ffect of nanoplexes on in vitro cell viability

Using the MTS assay, the cytotoxic effect of a 4 h exposure of BMSCs to nanoplexes containing 1 μg of *pDNA* at the N/P ratio of 10 was evaluated 48 h subsequent to exposure. The results showed > 93% of the BMSCs were viable after treatment with the nanoplexes (fig 2). Results of the one-way analysis of variance showed no significant difference in cell viabilities of treated versus non-treated cells. These data suggest that the PEI-*pDNA* nanoplexes were not toxic to the BMSCs cells after 48 h.

3.4. n vitro investigation of the combinatorial effect of PEI-(pBMP-2+pFGF-2) nanoplexes on gene expression

The ultimate aim of this research was to assess the *in vivo* synergistic effect of combining two encoded growth factors (BMP-2 and FGF-2) on stimulating bone regeneration. Such joint regulation can also be demonstrated *in vitro* by investigating the transgene nuclear delivery efficacy of the PEI-*pDNA* nanoplexes and quantifying the secretion of BMP-2 and FGF-2 protein from transfected cells. It has been demonstrated that FGF-2 and BMP-2 are important regulators of early and late stages of differentiation of osteoprogenitors, respectively [41]. FGF-2 induces its own expression as well as inducing genes that are associated with proliferation and angiogenesis, and is an essential regulator of migration, angiogenesis and proliferation during the early phase of bone healing and formation [42]. BMP-2 is the main growth factor involved in the late stage of bone healing (e.g. mineralization) and has no significant effect on genes associated with proliferation and angiogenesis. It has been shown that these two factors can synergistically enhance osteogenesis when given in appropriate doses through the SMAD/ERK signaling pathway, as well as through Runx2 phosphorylation. We have previously observed that combinatorial PEI-(*p*BMP-2+*p*FGF-2) treatment enhanced osteogenic differentiation and mineralization, as observed by alizarin red staining and atomic absorption spectroscopy, significantly more than each of the individual factors alone [28]. The BMP-2 ELISA test showed that the BMSCs transfected with PEI-(*p*BMP-2+*p*FGF-2) complexes secreted greater amounts of BMP-2 (approximately 2-fold higher) than cells treated with PEI-*pBMP-2* or PEI-*pFGF-2* alone (****$p < 0.0001$).

3.5. In vivo bone regeneration in diaphyseal long bone radial defects in a diabetic rabbit model: bone volume and union rate

Using a diabetic rabbit model with poor bone healing characteristics, the synergistic effect of collagen scaffolds containing PEI-(*pBMP-2*+*pFGF-2*) nanoplexes was evaluated *in vivo* by qualitative and quantitative assessments of bone repair. The *in vivo* efficacy of the ensuing groups was assessed: (1) defects filled with PEI-*pBMP-2* nanoplexes entrapped in collagen scaffolds, (2) defects filled with PEI-*pFGF-2* nanoplexes entrapped in collagen scaffolds, (3) defects filled with PEI-(*pBMP-2*+*pFGF-2*) nanoplexes entrapped collagen scaffolds. The rabbits were sacrificed after 28 days, the areas of interest were excised from the radial bone, and newly-formed bone tissue was assessed for its volume and union rate percentage using micro-computed tomography (μCT) scans.

Qualitatively, both on radiographs and μCT, there appeared to be increased callus formation in the combinatorial group (PEI-(*pBMP-2*+*pFGF-2*)) compared to the groups treated with PEI-*pBMP-2* or PEI-*pFGF-2* only (fig 4). Quantitatively, μCT scans revealed average bone volumes of 133.7 mm^3, 96.4 mm^3 and 82.2 mm^3 for defects treated with scaffolds containing PEI-(*pBMP-2*+*pFGF-2*)), PEI-*p*FGF-2 only and PEI-*p*BMP-2 only, respectively (fig 5a). There was significantly increased bone volume in the combinatorial (PEI-(*p*BMP-2+*p*FGF-2)) group compared to PEI-*p*BMP-2 group (P = 0.029, t-test). It has been shown previously that untreated defects in the size range of 1.4 to 2.0 cm display minimal irregular, patchy bone formation in healthy animal models at 12 weeks after fracture [43]. Bony union was considered complete when bridging bone between both cortices of the defect was observed. There was a significant increase in union rate in the combinatorial treatment (P = 0.033, chi-square test) compared to the group treated with PEI-*pBMP-2* only. Fracture union was found in 7 fractures (64%) of the combinatorial PEI-(*pBMP-2*+*pFGF-2*) group, 1 fracture (25%) in the PEI-*pFGF-2* group and 0 in PEI-*pBMP-2* group (fig 5b). The treatment groups were selected based on findings from research performed using a less challenging calvarial defect model (in healthy rodents) in which collagen scaffolds alone [33] and empty defects [32] failed to regenerate bone. Moreover, it has been previously shown that empty defects failed to regenerate bone in critical size rabbit radial defects [44]. We have found that gene-loaded matrices yield significantly enhanced bone regeneration in the calvarial model [32, 33]. In addition, since it was previously shown by our group that the combination of *pBMP-2* and *pFGF-2* treatment of adipose derived mesenchymal stem cells had a synergistic effect at promoting osteogenesis *in vitro*[28], we wished to test this combinatorial treatment in a more challenging diabetic diaphyseal bone regeneration model. Diabetes has a profoundly deleterious effect on bone healing as evidenced by delayed union and non-union after fracture[6].

3.6. In vivo bone regeneration in diaphyseal long bone radial defects in diabetic rabbit model: H&E and Masson's trichrome staining

Histology images stained with H&E and Masson's trichrome validated the μCT results. There was notably more bone area in the combinatorial PEI-(*pBMP-2*+*pFGF-2*) group compared to the PEI-*pBMP-2* only and PEI-*pFGF-2* only groups. There was no notable difference between the PEI-*p*BMP-2 only group and PEI-*p*FGF-2 only group in which bone did not bridge across the gap and defects remained unfilled. These two groups mostly

stimulated soft tissue regeneration with only small amounts of marginal bone formation. However, in the group treated with scaffolds embedded with the combinatorial PEI-(*p*BMP-2+*p*FGF-2) there was a complete bridging of the defect site by the mature bone tissue. (fig 6). It has been reported that delivery of PEI nanoplexes containing both *pBMP-2* and *pFGF-2* significantly enhanced the production of BMP-2 *in vitro* [28]. BMP-2 signaling is involved in bone matrix mineralization by promoting the secretion of the osteoid matrix that mineralizes to form mature bone tissue [45]. It is possible that the nanoplexes are gradually released from the collagen scaffold as it degrades, which are then free to transfect nearby cells. Cells co-transfected with *pBMP-2* and *pFGF-2* produce enhanced levels of BMP-2 which, along with FGF-2, stimulate osteoblastic cell migration into the collagen scaffold pores which can then result in the proliferation of endothelial cells and nascent blood vessel formation along with the recruitment into the scaffold of osteoprogenitors that subsequently differentiate [46].

4. Conclusion

We have shown for the first time, the synergistic effect of BMP-2 and FGF-2 on the regeneration of bone in rabbits with diabetes mellitus. Association of diabetes mellitus with delayed union and non-union after fracture makes this animal model more challenging for bone regeneration studies. The combination of BMP-2 and FGF-2 resulted in an effective bone regeneration response, as seen by segmental bone defects being completely reconstructed. The μCT results indicated that the group that received a combination of PEI (*pBMP-2* and *pFGF-2*) demonstrated increased bone mineral density as well as increased new bone formation in diaphyseal long bone radial defects compared to the treatments involving either PEI-*pBMP-2* or PEI-*pFGF-2*. Our data indicate combining *p*BMP-2 + *p*FGF-2 in nanoplexes and loading them into collagen scaffolds can enhance the bone repair and regeneration process. The synergistic effect of these bone inductive growth factors in combination with collagen scaffolds has the potential to be utilized for bone formation. In future studies, we intend to evaluate whether the sequence of delivery of *p*BMP-2 and *p*FGF-2 can be used to optimize the level of new bone formed and we intend to investigate the optimal ratio between these two genes. Our ultimate goal is to move this delivery system into the clinic.

Acknowledgments

This research was supported by a grant from the American Orthopaedic Foot & Ankle Society and the Lyle and Sharon Bighley Professorship.

References

[1]. Graves DT, Alblowi J, Paglia DN, O'Connor JP, Lin S. Impact of Diabetes on Fracture Healing. Journal of Experimental & Clinical Medicine. 2011; 3:3–8.

[2]. McNair P, Madsbad S, Christensen MS, Christiansen C, Faber OK, Binder C, Transbol I. Bone mineral loss in insulin-treated diabetes mellitus: studies on pathogenesis. Acta Endocrinol. (Copenh.). 1979; 90:463–472. [PubMed: 425786]

[3]. McNair P, Christiansen C, Christensen MS, Madsbad S, Faber OK, Binder C, Transbol I. Development of bone mineral loss in insulin-treated diabetes: a 1 1/2 years follow-up study in sixty patients. Eur. J. Clin. Invest. 1981; 11:55–59. [PubMed: 6783430]

[4]. Vestergaard P. Discrepancies in bone mineral density and fracture risk in patients with type 1 and type 2 diabetes--a meta-analysis. Osteoporos. Int. 2007; 18:427–444. [PubMed: 17068657]

[5]. Papa J, Myerson M, Girard P. Salvage, with arthrodesis, in intractable diabetic neuropathic arthropathy of the foot and ankle. J. Bone Joint Surg. Am. 1993; 75:1056–1066. [PubMed: 8335665]

[6]. Loder RT. The influence of diabetes mellitus on the healing of closed fractures. Clin. Orthop. Relat. Res. 1988:210–216.

[7]. Gandhi A, Beam HA, O'Connor JP, Parsons JR, Lin SS. The effects of local insulin delivery on diabetic fracture healing. Bone. 2005; 37:482–490. [PubMed: 16027060]

[8]. Hou JC, Zernicke RF, Barnard RJ. Experimental diabetes, insulin treatment, and femoral neck morphology and biomechanics in rats. Clin. Orthop. Relat. Res. 1991:278–285.

[9]. Reddy GK, Stehno-Bittel L, Hamade S, Enwemeka CS. The biomechanical integrity of bone in experimental diabetes. Diabetes Res. Clin. Pract. 2001; 54:1–8. [PubMed: 11532324]

[10]. Durmuşlar MC, Ballı U, Öngöz Dede F, Bozkurt Doğan Ş, Mısır AF, Barış E, Yılmaz Z, Çelik HH, Vatansever A. Evaluation of the effects of platelet-rich fibrin on bone regeneration in diabetic rabbits. Journal of Cranio-Maxillofacial Surgery. 2016; 44:126–133. [PubMed: 26732635]

[11]. Cozen L. Does diabetes delay fracture healing? Clin. Orthop. Relat. Res. 1972; 82:134–140. [PubMed: 5011018]

[12]. Kayal RA, Tsatsas D, Bauer MA, Allen B, Al-Sebaei MO, Kakar S, Leone CW, Morgan EF, Gerstenfeld LC, Einhorn TA, Graves DT. Diminished bone formation during diabetic fracture healing is related to the premature resorption of cartilage associated with increased osteoclast activity. J. Bone Miner. Res. 2007; 22:560–568. [PubMed: 17243865]

[13]. Schultz O, Sittinger M, Haeupl T, Burmester GR. Emerging strategies of bone and joint repair. Arthritis Res. Ther. 2000; 2:1–4.

[14]. Azad V, Breitbart E, Al-Zube L, Yeh S, O'Connor JP, Lin SS. rhBMP-2 enhances the bone healing response in a diabetic rat segmental defect model. J. Orthop. Trauma. 2009; 23:267–276. [PubMed: 19318870]

[15]. Kawaguchi H, Kurokawa T, Hanada K, Hiyama Y, Tamura M, Ogata E, Matsumoto T. Stimulation of fracture repair by recombinant human basic fibroblast growth factor in normal and streptozotocin-diabetic rats. Endocrinology. 1994; 135:774–781. [PubMed: 8033826]

[16]. Naganawa T, Xiao L, Abogunde E, Sobue T, Kalajzic I, Sabbieti M, Agas D, Hurley MM. In vivo and in vitro comparison of the effects of FGF-2 null and haplo-insufficiency on bone formation in mice. Biochem. Biophys. Res. Commun. 2006; 339:490–498. [PubMed: 16298332]

[17]. Khan SN, Lane JM. The use of recombinant human bone morphogenetic protein-2 (rhBMP-2) in orthopaedic applications. Expert Opin. Biol. Ther. 2004; 4:741–748. [PubMed: 15155165]

[18]. Seo B-B, Choi H, Koh J-T, Song S-C. Sustained BMP-2 delivery and injectable bone regeneration using thermosensitive polymeric nanoparticle hydrogel bearing dual interactions with BMP-2. J. Control. Release. 2015; 209:67–76. [PubMed: 25910579]

[19]. Chen G, Deng C, Li Y-P. TGF-β and BMP Signaling in Osteoblast Differentiation and Bone Formation. Int. J. Biol. Sci. 2012; 8:272–288. [PubMed: 22298955]

[20]. Derynck R, Zhang Y, Feng XH. Smads: transcriptional activators of TGF-beta responses. Cell. 1998; 95:737–740. [PubMed: 9865691]

[21]. Reddi AH, Huggins C. Biochemical Sequences in the Transformation of Normal Fibroblasts in Adolescent Rats. Proceedings of the National Academy of Sciences. 1972; 69:1601–1605.

[22]. Kouhara H, Hadari YR, Spivak-Kroizman T, Schilling J, Bar-Sagi D, Lax I, Schlessinger J. A lipid-anchored Grb2-binding protein that links FGF-receptor activation to the Ras/MAPK signaling pathway. Cell. 1997; 89:693–702. [PubMed: 9182757]

[23]. Marshall CJ. Specificity of receptor tyrosine kinase signaling: transient versus sustained extracellular signal-regulated kinase activation. Cell. 1995; 80:179–185. [PubMed: 7834738]

[24]. Marie PJ, Debiais F, Hay E. Regulation of human cranial osteoblast phenotype by FGF-2, FGFR-2 and BMP-2 signaling. Histol. Histopathol. 2002; 17:877–885. [PubMed: 12168799]

[25]. Ducy P, Zhang R, Geoffroy V, Ridall AL, Karsenty G. Osf2/Cbfa1: a transcriptional activator of osteoblast differentiation. Cell. 1997; 89:747–754. [PubMed: 9182762]

[26]. Bruderer M, Richards RG, Alini M, Stoddart MJ. Role and regulation of RUNX2 in osteogenesis. European cells & materials. 2014; 28:269–286. [PubMed: 25340806]

[27]. Hayashi H, Ishisaki A, Suzuki M, Imamura T. BMP-2 augments FGF-induced differentiation of PC12 cells through upregulation of FGF receptor-1 expression. J. Cell Sci. 2001; 114:1387–1395. [PubMed: 11257004]

[28]. Atluri K, Seabold D, Hong L, Elangovan S, Salem AK. Nanoplex-Mediated Codelivery of Fibroblast Growth Factor and Bone Morphogenetic Protein Genes Promotes Osteogenesis in Human Adipocyte-Derived Mesenchymal Stem Cells. Mol. Pharm. 2015; 12:3032–3042. [PubMed: 26121311]

[29]. D'Mello S, Atluri K, Geary SM, Hong L, Elangovan S, Salem AK. Bone Regeneration Using Gene-Activated Matrices. The AAPS journal. 2016

[30]. Shimer AL, Öner FC, Vaccaro AR. Spinal reconstruction and bone morphogenetic proteins: Open questions. Injury. 2009; 40(Supplement 3):S32–S38. [PubMed: 20082788]

[31]. Winn SR, Hu Y, Sfeir C, Hollinger JO. Gene therapy approaches for modulating bone regeneration. Advanced drug delivery reviews. 2000; 42:121–138. [PubMed: 10942818]

[32]. Elangovan S, Khorsand B, Do A-V, Hong L, Dewerth A, Kormann M, Ross RD, Rick Sumner D, Allamargot C, Salem AK. Chemically modified RNA activated matrices enhance bone regeneration. J. Control. Release. 2015; 218:22–28. [PubMed: 26415855]

[33]. Elangovan S, D'Mello SR, Hong L, Ross RD, Allamargot C, Dawson DV, Stanford CM, Johnson GK, Sumner DR, Salem AK. The enhancement of bone regeneration by gene activated matrix encoding for platelet derived growth factor. Biomaterials. 2014; 35:737–747. [PubMed: 24161167]

[34]. D'Mello S, Salem AK, Hong L, Elangovan S. Characterization and evaluation of the efficacy of cationic complex mediated plasmid DNA delivery in human embryonic palatal mesenchyme cells. J. Tissue Eng. Regen. Med. 2014 n/a-n/a.

[35]. Wang J, Wan R, Mo Y, Zhang Q, Sherwood LC, Chien S. Creating a Long-Term Diabetic Rabbit Model. Exp. Diabetes Res. 2010; 2010:289614. [PubMed: 21234414]

[36]. Wagner E, Cotten M, Foisner R, Birnstiel ML. Transferrin-polycation-DNA complexes: the effect of polycations on the structure of the complex and DNA delivery to cells. Proceedings of the National Academy of Sciences. 1991; 88:4255–4259.

[37]. Boussif O, Lezoualc'h F, Zanta MA, Mergny MD, Scherman D, Demeneix B, Behr JP. A versatile vector for gene and oligonucleotide transfer into cells in culture and in vivo: polyethylenimine. Proceedings of the National Academy of Sciences. 1995; 92:7297–7301.

[38]. Godbey WT, Wu KK, Mikos AG. Poly(ethylenimine) and its role in gene delivery. J. Control. Release. 1999; 60:149–160. [PubMed: 10425321]

[39]. Perez RA, Seo S-J, Won J-E, Lee E-J, Jang J-H, Knowles JC, Kim H-W. Therapeutically relevant aspects in bone repair and regeneration. Materials Today. 2015; 18:573–589.

[40]. Putnam AJ, Mooney DJ. Tissue engineering using synthetic extracellular matrices. Nat. Med. 1996; 2:824–826. [PubMed: 8673932]

[41]. Hughes-Fulford M, Li CF. The role of FGF-2 and BMP-2 in regulation of gene induction, cell proliferation and mineralization. J. Orthop. Surg. Res. 2011; 6:8. [PubMed: 21306641]

[42]. Barati D, Shariati SRP, Moeinzadeh S, Melero-Martin JM, Khademhosseini A, Jabbari E. Spatiotemporal release of BMP-2 and VEGF enhances osteogenic and vasculogenic differentiation of human mesenchymal stem cells and endothelial colony-forming cells co-encapsulated in a patterned hydrogel. J. Control. Release. 2016; 223:126–136. [PubMed: 26721447]

[43]. Zhao M-D, Huang J-S, Zhang X-C, Gui K-K, Xiong M, Yin W-P, Yuan F-L, Cai G-P. Construction of Radial Defect Models in Rabbits to Determine the Critical Size Defects. PLoS One. 2016; 11:e0146301. [PubMed: 26731011]

[44]. Geiger F, Bertram H, Berger I, Lorenz H, Wall O, Eckhardt C, Simank HG, Richter W. Vascular endothelial growth factor gene-activated matrix (VEGF165-GAM) enhances osteogenesis and angiogenesis in large segmental bone defects. J. Bone Miner. Res. 2005; 20:2028–2035. [PubMed: 16234976]

[45]. Seib FP, Franke M, Jing D, Werner C, Bornhäuser M. Endogenous bone morphogenetic proteins in human bone marrow-derived multipotent mesenchymal stromal cells. Eur. J. Cell Biol. 2009; 88:257–271. [PubMed: 19303661]

[46]. Saran U, Gemini Piperni S, Chatterjee S. Role of angiogenesis in bone repair. Arch. Biochem. Biophys. 2014; 561:109–117. [PubMed: 25034215]

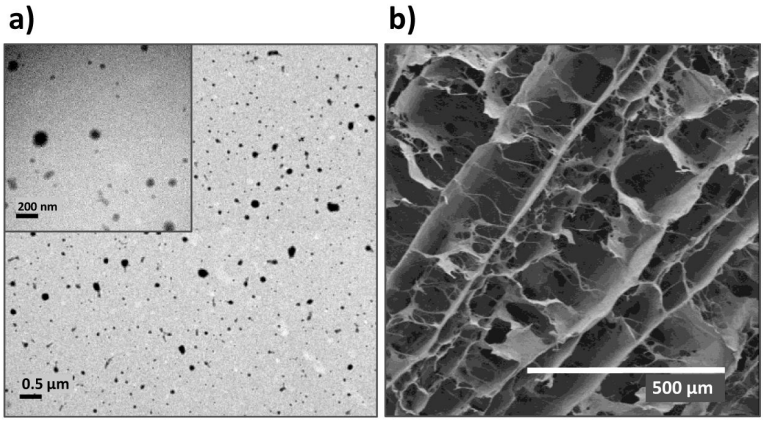

Fig.1.

(a) TEM images of PEI-(*p*BMP-2+*p*FGF-2) nanoplexes prepared at the N/P ratio of 10 (scale bar = 0.5 µm; inset scale bar = 200 nm). **(b)** SEM images of collagen scaffolds (scale bar = 500 µm).

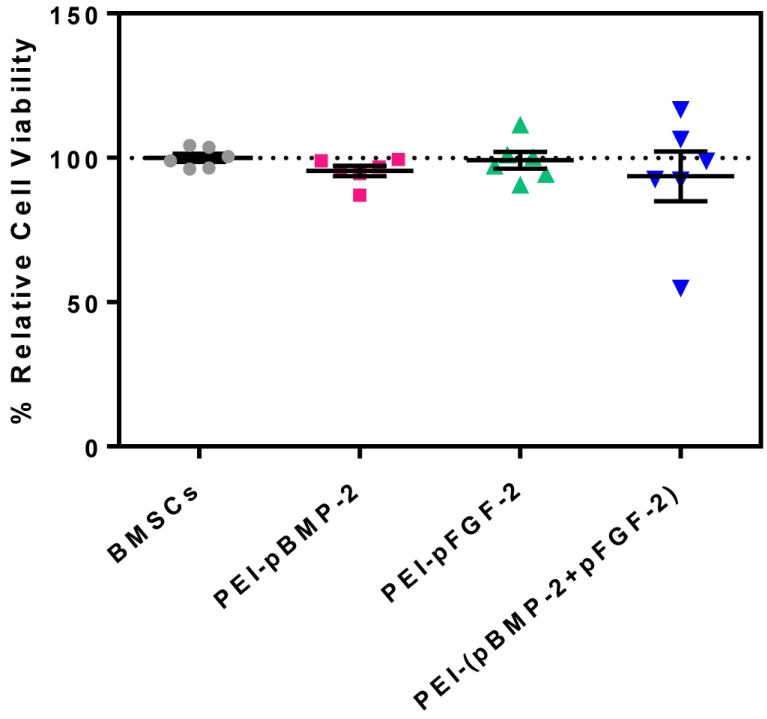

Fig.2.

Cytotoxicity of PEI-*p*DNA nanoplexes fabricated at the N/P ratio of 10 (1 μg *p*DNA) in BMSCs using an MTS assay 48 h subsequent to treatment. Values are expressed as mean ± SEM (n = 6).

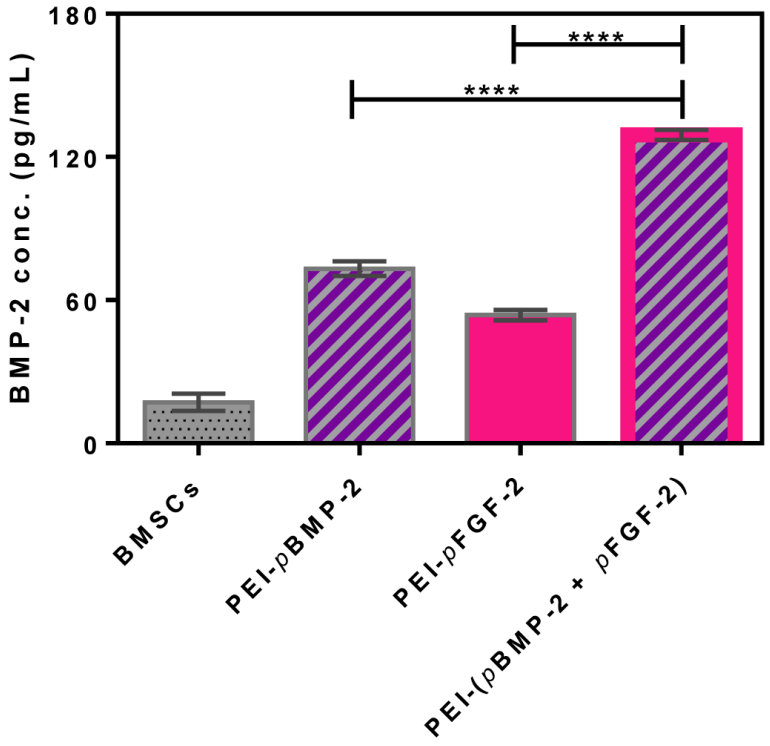

Fig.3.

ELISA assay demonstrating the transfection efficiency of the indicated nanoplexes and the expression levels of BMP-2 protein by BMSCs at 48 h post transfection. ****$p < 0.0001$. Values are expressed as mean ± SEM ($n = 4$).

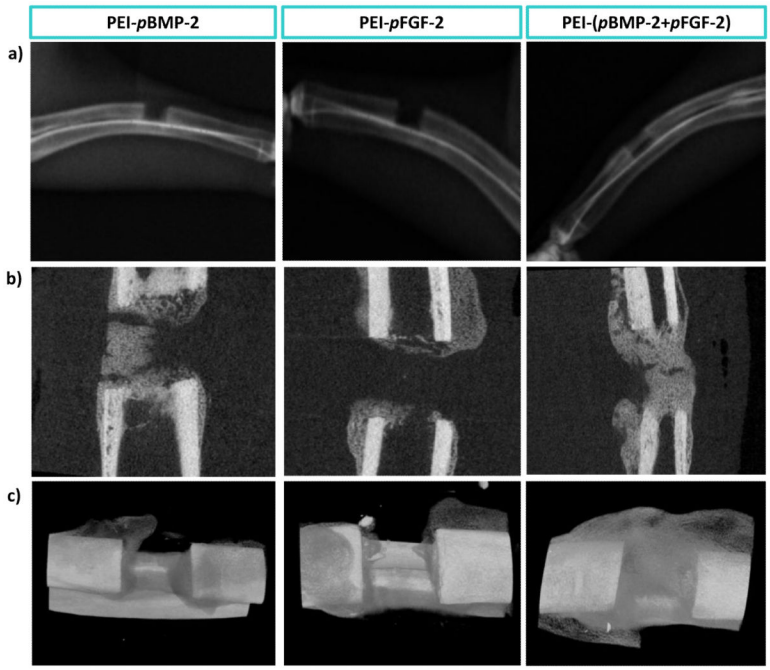

Fig.4.

Qualitative bone repair; Representative μCT **(a)** scout view, **(b)** sagittal slices, and **(c)** 3-D reconstruction through defects demonstrating the level of regenerated bone tissue after 28 days of treatment with: scaffolds embedded with PEI-*pBMP-2* nanoplexes; PEI-*pFGF-2* nanoplexes**;** or PEI-(*pBMP-2*+*pFGF-2*) nanoplexes.

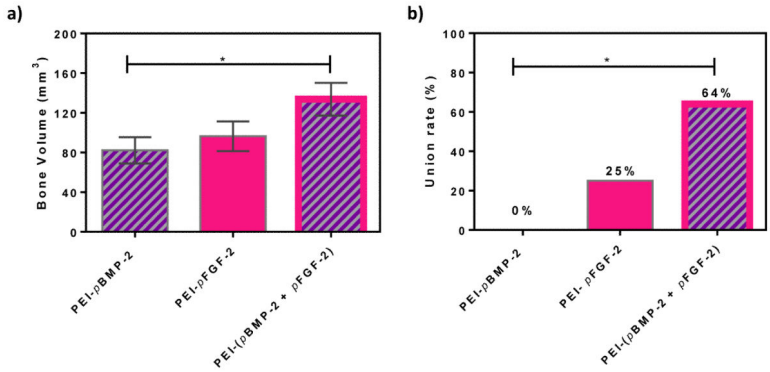

Fig.5.

Quantitative bone repair (a) Bone volume and **(b)** union rate of regenerated bone after 28 days. Significant differences between treatments were assessed by t-test for comparing the bone volume and chi-square test for the union rates (*$p < 0.05$). (Values are expressed as mean ± SEM)

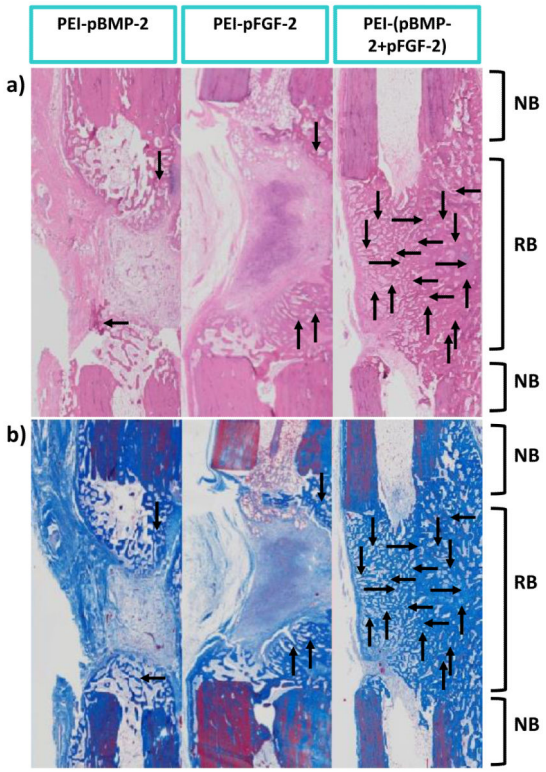

Fig.6.

Images of histology sections indicating the degree of nascent bone formation at the defect sites at 28 days in response to indicated treatments. Representative histology sections after **(a)** H&E, and **(b)** Masson's trichrome staining. As shown, there is qualitatively more bone area in the combination PEI-(*p*BMP-2+*p*FGF-2) group compared to the PEI-*pBMP-2* or PEI-*pFGF-2* only. NB-native bone and RB-regenerated bone. Note the complete bridging of new bone (indicated by the arrows) in the group treated with scaffolds embedded with PEI-(*p*BMP-2+*p*FGF-2) nanoplexes.

Table 1

Size and Zeta Potential of nanoplexes prepared at N/P Ratio 10

Nanoplexes	Z-Ave (d. nm.) ± SEM	PDI ± SEM	Zeta Potential (mV)± SEM
PEI-*pBMP-2*	83.4 ± 0.8	0.03 ± 0.01	34.9 ± 0.3
PEI-*pFGF-2*	90.5 ± 1.4	0.13 ± 0.02	35.6 ± 0.2
PEI-(*pBMP-2*+*pFGF-2*)	116.4 ± 1.1	0.08 ± 0.03	30.3 ± 0.3